Non-linear interaction between tidal and subinertial barotropic flows in the Strait of Gibraltar

Barotropic flow
Subinertial flow
Tide in channel
Non-linear interaction
Strait of Gibraltar

Flux barotrope
Flux subinertiel
Marée dans un canal
Interaction non linéaire
Détroit de Gibraltar

Rafael MAÑANES, M. BRUNO, J. ALONSO, B. FRAGUELA and L. TEJEDOR

Facultad de Ciencias del Mar. Polígono del Río San Pedro S/n. Apartado 40. Puerto Real. Cádiz, Spain.

Received 17/12/96, in revised form 01/04/97, accepted 30/04/97.

ABSTRACT

The present work establishes clear relationships of the amplitude and phase variation of the barotropic M_2 signal in the velocity of the current with the barotropic subinertial flow in the Strait of Gibraltar. The analytical procedure is applied on data from Gibraltar Experiment in order to obtain barotropic subinertial series and the amplitude and phase variation of the M_2 signal series involves harmonic analysis, empirical orthogonal function analysis and complex demodulation. In addition, cross-spectral analysis has been applied to study these relationships, concerning which non-linear interaction between M_2 and the subinertial oscillation is proposed as the responsible physical mechanism. An analytical solution characterizing this type of non-linear interaction is offered in explanation of the experimental results. © Elsevier, Paris.

RÉSUMÉ

Interaction non linéaire entre les flux barotropes de marée et subinertiel dans le détroit de Gibraltar.

Le présent travail établit les relations entre l'amplitude et les variations de phase du signal barotrope M_2 dans le détroit de Gibraltar et le flux barotrope subinertiel. Les séries de données sont traitées par un ensemble de méthodes : analyse harmonique, analyse des fonctions orthogonales empiriques, démodulation complexe et analyse spectrale croisée. Le mécanisme physique responsable des relations entre le signal M_2 et l'oscillation subinertielle est l'interaction non linéaire. Une solution analytique de ce type d'interaction explique des résultats expérimentaux. © Elsevier, Paris.

Oceanologica Acta, 1998, **21**, 1, 33-46.

INTRODUCTION

From the oceanographic point of view, the Strait of Gibraltar is known to play an important role in controlling the exchange of water masses between the Mediterranean Sea and the Atlantic Ocean. On a stationary scale, the responsible mechanisms for moving these water masses are the density and mean sea level differences between both basins mainly. Over this stationary structure, other water mass movements with different temporal variability scales are found. According to their temporal scales the flows in the Strait of Gibraltar can be classified (Lacombe and Richez, 1982) as: long-period, subinertial and tidal.

The forcing mechanism of subinertial flows has been investigated by different authors and related to atmospheric pressure fluctuations over the Mediterranean Sea (Crepon, 1965; Garrett, 1983; García, 1986; Candela, 1989; Candela *et al.*, 1989). Estimated low-frequency variability transports are 0.37 and 0.22 Sv for Atlantic inflow and Mediterranean outflow respectively (Bryden *et al.*, 1994).

The tidal flow in the Strait is the result of the coupling between the Atlantic and Mediterranean tidal regimes (García, 1986; Candela, 1989; Ruíz, 1994). The estimated tidal transports are 2.3 and 1.3 Sv for inflow and outflow respectively (Bryden *et al.*, 1994).

The tidal and subinertial flows can be considered almost unidirectional, with a clear predominance of the west–east component of the current velocity "u" over the south–north component "v" (Pillsbury *et al.*, 1987).

An important feature of the tidal and subinertial flows is that they can be considered, as a first approach, as barotropic, *i.e.* depth-independent. Candela (1989) and Ruíz (1994) have found that 93 and 84 %, respectively, of the variance of current velocities in semidiurnal and subinertial bands have a barotropic character in the Strait of Gibraltar. The M_2 signal explains over 64 % of the tidal barotropic flow variance (Candela, 1989; Candela *et al.*, 1990) and can therefore be used to characterize a very important part of the tidal phenomenon in the Strait.

One of the pending subjects of oceanographic studies in the Strait of Gibraltar is the analysis of non-linear phenomena affecting tidal and subinertial oscillations. Several authors have studied this problem in connection with sea elevation records taken along the Strait (García, 1986; Garrett *et al.*, 1989; Mañanes *et al.*, 1995). The present work establishes clear relationships of the amplitude and phase-lag variation of the barotropic M_2 signal in the velocity of the current with the barotropic subinertial current in the Strait of Gibraltar. These relationships will be explained, taking as a basis the non linear interactions between M_2 and the subinertial signals in the current velocity.

The organization of the paper is as follows. The first part describes data records and their processing in order to obtain the barotropic subinertial oscillation mode and the amplitude and phase variation of the M_2 barotropic signal. In the second part, the relationship between the series already described is established and discussed. The third part is devoted to semidiurnal residues and their spatial variations along the Strait. In the fourth part, the non-linear interaction between M_2 and subinertial oscillation is proposed as the physical mechanism responsible for the generation of the semidiurnal residues. A quasi-analytical solution characterizing this kind of non-linear interaction is used to explain the experimental results. In the fifth and final part, the comparison between the observed and theoretical results is discussed.

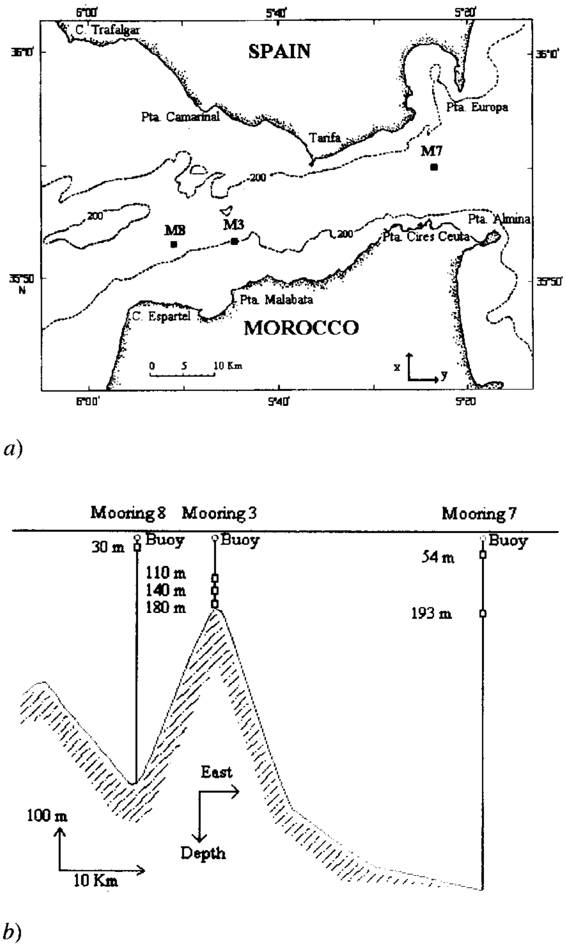

Figure 1

a) Map of the studied zone, with the location of the selected moorings M8, M3 and M7; b) detail of the selected moorings.

DATA AND METHODOLOGY

Current velocity data were obtained from the Gibraltar Experiment (1985–1986). Not all the moorings available in this experiment were used, but only those which met the following conditions: they must be located close to the longitudinal axis of the Strait, and be well separated from each other; and they must be the subject of the longest simultaneous period of recordings. On the basis of these criteria, moorings M8, M3 and M7 were selected (Fig. 1*a*). The longest simultaneous record comprised about three months of hourly data (Table 1).

The purpose now is to determine the series which represent, on the one hand, the barotropic subinertial signal and, on the other hand, the amplitude and phase variations of the barotropic M_2 signal in the velocity data of the current. It will be found that the barotropic subinertial signal can be represented by a common oscillation mode along the entire Strait which will be characterized by its temporal weight $M_1(t)$. After the distorted M_2 signal is obtained, the slow variations in time of the amplitude and phase of the M_2 signal are computed by the application of complex demodulation to the distorted M_2 signal. These slow variations in time of amplitude and phase have been called $U_m(t)$ and $\phi_m(t)$, respectively, and are determined together with $M_1(t)$, for use in the next section to analyse the relationship of $M_1(t)$ with $U_m(t)$ and $\phi_m(t)$.

Table 1

Information concerning the moorings M3, M8 and M7 used in the present work.

Moorings	Water Depth (m)	Latitude	Longitude	Start	Stop	Depth of instrument (m)
M3	190 m	35°53.42'	05°44.20'	21/10/85	21/4/86	110 m
				21/10/85	21/4/86	140 m
				21/10/85	21/4/86	180 m
M7	916 m	35°59.98'	05°22.75'	19/10/85	27/3/86	54 m
				19/10/85	27/3/86	193 m
M8	610 m	35°53.16'	05°50.55'	17/10/85	26/3/86	30 m

To obtain the barotropic semidiurnal signal at each mooring, the following procedure was followed:

Empirical orthogonal function analysis (EOF) (Kundu *et al.*, 1975; Kundu and Allen, 1976; Candela, 1989; Bruno *et al.*, 1996*b*) was applied to the original current velocity series to obtain the total barotropic signal. Since there was only one current meter at a depth of 30 metres at M8 (Fig. 1*b*) it had to be assumed that the recorded signal was the barotropic one. Results of the EOF at moorings M3 and M7 are shown in Tables 2*a* and 2*b*, respectively, where mode 1, showing the same sign in the spatial weights (eigenvectors) for all current meters and approximately constant values with depth, is the most energetic one, and can be understood as a close approximation to the barotropic mode. These results agree with those obtained by Candela (1989) for the tidal barotropic mode (*see* values in brackets in Table 2).

Table 2

*Results of EOF application to the original hourly data of current meters. a) At mooring M3; b) at mooring M7. * means for percentage of variance explained for each mode in each of the current meters. ** means for total percentage of variance explained for each mode. Values obtained by Candela (1989) for mooring M3 are shown between brackets.*

a)

Mode	Eigenvectors			Variance*			Var**
	C3110	C3140	C3180	C3110	C3140	C3180	Total
1°	82.0 (92.6)	71.2 (83.6)	46.5 (55.8)	99.6	99.7	97.4	99.31
2°	−3.9	−0.3	−4.1	0.2	0.00	0.3	0.50
3°	2.9	−4.1	1.3	0.1	0.3	0.08	0.19

b)

Mode	Eigenvectors		Variance*		Var**
	C754	C7193	C754	C7193	Total
1°	16.3	23.4	54.3	81.6	69.7
2°	−15.4	11.1	45.7	18.4	30.3

The Fast Fourier Transform filter on the total barotropic signal was applied to the isolate barotropic semidiurnal signal on each mooring. Once this signal was obtained, a least-squares harmonic analysis (Foreman, 1976) was applied to estimate the harmonic constants for the main semidiurnal tidal constituents. These constants are presented in Table 3 for the three selected moorings.

Once the barotropic semidiurnal signal was obtained, the $U_m(t)$ and $\phi_m(t)$ series were obtained as follows.

A prediction without the M_2 constituent was generated using the constants of Table 3 and subtracted from the barotropic semidiurnal signal. The resulting signal was thus composed of the M_2 signal plus the semidiurnal residue, and can be understood as a distorted M_2 signal which can be characterized by the expression:

$$u^d_{M2}(t) = U_m(t)\cos\left[\omega_{M2}t - \phi_m(t)\right] \qquad (1)$$

where $u^d_{M2}(t)$ is the distorted M_2 signal and $U_m(t)$ and $\phi_m(t)$ are the slow variations in time of the amplitude and phase lag of the M_2 signal. It should be noted that the semidiurnal residue contains not only the distortion effects felt by the M_2 signal but also those felt by the other semidiurnal constituents. However, considering that the M_2 constituent accounts over 64 % of the variance contained in the semidiurnal band, the distortion of the total semidiurnal signal can be basically represented the distortion of the M_2 signal. Hence the signal given in equation (1) is called the distorted M_2 signal.

Table 3

Harmonic constants estimation of the tidal barotropic semidiurnal signal in the current velocity at the moorings M8, M3 and M7. A is the amplitude in cm s^{-1} and G is the Greenwich phase lag in degrees.

Component	Period (hours)	Mooring 8		Mooring 3		Mooring 7	
		A	G	A	G	A	G
ε_2	13.12	1.58	117.3	0.71	123.9	1.27	72.6
μ_2	12.87	3.29	138.5	0.33	59.8	4.10	110.7
N_2	12.65	14.98	134.6	17.87	120.9	6.80	129.9
M_2	12.42	65.15	156.5	90.83	146.6	24.85	159.5
L_2	12.19	1.37	154.3	2.46	171.3	2.67	310.9
S_2	11.99	22.60	185.1	30.70	170.5	12.43	177.9
K_2	11.96	6.78	185.8	9.21	171.2	3.73	178.6
η_2	11.75	0.65	97.4	0.91	18.6	0.30	331.7

Next, the $U_m(t)$ and $\phi_m(t)$ series were obtained by the application of complex demodulation at the M_2 frequency to the series $u^d_{M2}(t)$ (Korn and Korn, 1986; Garrett *et al.*, 1989; Bruno *et al.*, 1996*a*; Mañanes, 1996).

Table 4

*Results of EOF application to the subinertial signal of current meters at moorings M3, M8 and M7. * means for percentage of variance explained for each mode in each of the current meters. ** means for total percentage of variance explained for each mode. Values obtained by Candela (1989) for mooring M3 are shown between brackets.*

Mode	Eigenvectors					Variance*					Var**
	C3110	C3140	C3180	C7193	C830	C3110	C3140	C3180	C7193	C830	Total
1°	16.8	16.5	11.2	4.6	5.3	93.5	97.3	83.2	54.1	38.6	86.3
	(17.3)	(17.4)	(12.0)								(80.0)
2°	-2.7	1.4	4.1	1.5	-5.6	2.4	0.7	11.0	6.1	43.2	7.1
3°	3.3	-0.3	-2.4	-0.8	-3.7	3.6	0.0	4.0	1.9	18.2	3.7
4°	0.6	-1.3	-0.5	3.8	0.1	0.1	0.6	0.2	37.0	0.0	2.0
5°	1.0	-1.9	1.6	-0.6	0.1	0.3	1.4	1.7	0.9	0.0	0.9

The barotropic subinertial signal was obtained as follows:

The moving average filter $A_{24}\,A_{24}\,A_{25}$ (Godin, 1972), which has a cut frequency of 0.033 cycles/hour corresponding to a period of 30 hours, was applied to the original hourly data yielding the subinertial signal at all the current meters.

EOF is applied on the subinertial signal of all current meters in order to seek a common mode characterizing the barotropic subinertial oscillation along the Strait. Current meter C754, located at mooring M7 at a depth of 54 m (Fig. 1*b*), was not included in the analysis because of its anomalous behaviour with respect to the other current meters deployed in the Gibraltar Experiment. In this current meter, the subinertial signal accounted for 53 % of the total variance, while the characteristic percentage of the variance explained by the subinertial signal in the others was 6 % (Candela, 1989; Candela *et al.*, 1990). The results of the EOF analysis are presented in Tables 3 and 4, where it should be noted that the spatial weights of mode 1 show the same sign for all the current meters and the spatial weights associated to this mode are nearly uniform with depth at the M3 mooring, which was therefore chosen as the representative barotropic subinertial mode and called $M_1\,(t)$. Results follow those obtained by Candela (1989) and Candela *et al.* (1989) for barotropic subinertial mode in M3 (*see* values between brackets in Table 4).

RELATIONSHIP BETWEEN AMPLITUDE AND PHASE VARIATION OF THE M_2 SIGNAL AND SUBINERTIAL BAROTROPIC MODE

The $U_m\,(t)$, $\phi_m\,(t)$ and $M_1\,(t)$ series having been obtained, the relationships between both amplitude and phase variation of the M_2 signal in the barotropic current velocity, and the barotropic subinertial mode were analyzed for each of the moorings used.

In Figure 2, certain relationships between both pairs of series ($M_1\,(t)$ with $U_m\,(t)$ and $\phi_m\,(t)$) can be observed. To look into this relationship a cross-spectral analysis between both pairs of series was performed. Results from these analyses for each mooring are shown in Figures 3–5. From Figures 3–5*a* and 3–5*b* it can be seen that in the frequency range where the explained percentage of energy is higher for all series (from 0.0432 to 0.1296 cycles/day), the coherence shows significant values, between 0.5 and 0.8, implying a significant correlation of the two pairs of series at all moorings. From Figures 3*c* and 4*c* and Figures 3*d* and 4*d*, the phase lag between $M_1\,(t)$ and both $U_m\,(t)$ and $\phi_m\,(t)$ series is a function of the frequency at all moorings, yet in the frequency range where the explained percentage of energy is higher its value is located, in the case of $U_m\,(t)$, between 90 and 180 ° for all moorings and, in the case of $\phi_m\,(t)$, between 180 and 270 ° at moorings M8 and M3 and close to 360 ° at mooring M7. Thus the relationships between the barotropic subinertial mode and both amplitude and phase variation of the M_2 signal show a greater similarity of behaviour between the moorings at the western side of the Strait (M8 and M3) than between these and the mooring at the eastern side (M7). This can be explained by the different dynamic conditions existing on each side of the Strait.

SEMIDIURNAL RESIDUES IN THE CURRENT VELOCITY ALONG THE STRAIT AS A FUNCTION OF SLOW VARIATIONS IN TIME OF AMPLITUDE AND PHASE OF M_2 SIGNAL

The semidiurnal residue in the barotropic current velocity is defined as

$$u_r\,(t) = u^d_{M2}\,(t) - U_{M2}\cos\left(\omega_{M2}\,t - \delta_{uM2}\right) \quad (2)$$

where $u^d_{M2}\,(t)$ is given by equation (1); U_{M2} and δ_{uM2} are the estimated harmonic constants, amplitude and phase, of the M_2 signal in the current velocity; and ω_{M2} is the angular frequency of the M_2 signal. The $u^d_{M2}\,(t)$ series in equation (2) can be expressed (Bruno *et al.*, 1996*a*) as:

$$u^d_{M2}\,(t) = U_{M2}\,U_t\cos\left(\omega_{M2}\,t - \delta_{uM2}\,\phi_t\right) \quad (3)$$

where:

$$U_t = \frac{U_m\,(t)}{U_{M2}}$$

$$\phi_t = \frac{\phi_m\,(t)}{\delta_{uM2}}$$

are nondimensional factors which express the proportion of amplitude and phase variations with respect to the harmonic constants for the M_2 constituent. Developing equation (3)

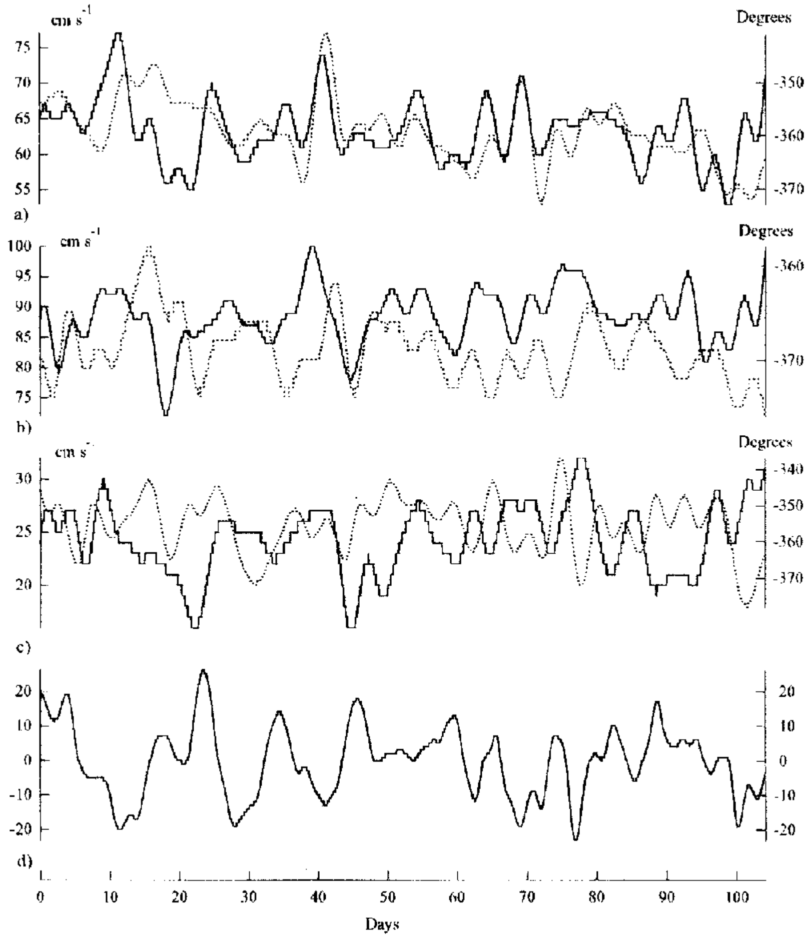

Figure 2

M_2 signal amplitude and phase distortion series in current velocity, $U_m(t)$ (solid lines) and $\phi_m(t)$ (dotted lines) at: a) M8; b) M3; c) M7; d) barotropic subinertial mode $M_1(t)$.

as a function of U_t and ϕ_t by Taylor's series around the undistorted signal ($U_t = 1$ and $\phi_t = 1$) and truncating it in the first order (Bruno *et al.*, 1996*a*; Mañanes, 1996) results in

$$u^d_{M2}(t) = u^d_{M2}(1,1) + \frac{\partial u^d_{M2}}{\partial U_t}|_{(1,1)}(U_t - 1) + \frac{\partial u^d_{M2}}{\partial \phi_t}|_{(1,1)}(\phi_t - 1) \quad (4)$$

Evaluating the partial derivatives in $U_t = 1$ and $\phi_t = 1$, and taking in account that

$$u^d_{M2}(t)(1,1) = U_{M2}\cos(\omega_{M2}t - \delta_{u_{M2}})$$

in equation (4) we obtain

$$u_r(t) = u^d_{M2}(t) - U_{M2}\cos(\omega_{M2}t - \delta_{u_{M2}}) \approx U_{M2}\cos(\omega_{M2}t - \delta_{u_{M2}})(U_t - 1) + \delta_{uM2}U_{M2}\sin(\omega_{M2}t - \delta_{u_{M2}})(\phi_t - 1) \quad (5)$$

The right-hand side of equation (5) can then be considered as an approximation to the semidiurnal residue $u_r(t)$. Figure 6 shows the residual series estimated from equation (2) (Fig. 6*a*) and its approximation from equation (5) (Fig. 6*b*), for mooring M3, during the analyzed period. Also, the differences between the residue and its approximation (Fig. 6*c*) are shown. In Table 5 it should be noted that the quotient between the standard deviations of the series in Figure 6*c* and the series in Figure 6*a* is 0.0839, and therefore the approximation to the semidiurnal residue by equation (5) is quite satisfactory.

From equation (5), the residual variance can be divided into two parts, of which the first one is proportional to the M_2 signal

$$u_{r_1} = C_0\cos(\omega_{M2}t - \delta_{uM2}) \quad (6)$$

Table 5

Standard deviation of semidiurnal residues at moorings M8, M3 and M7: σ_{ur} for the residue from equation (2); σ_{ura} for the residue approximation equation (5); σ_{ur1} for the contribution to the semidiurnal residue from the M_2 signal amplitude variation; σ_{ur2} for the contribution to the semidiurnal residue from the M_2 signal phase variation; and σ_{DIF} for the difference between the observed and the approximated residue.

Mooring	σ_{ur} (m s^{-1})	σ_{ura} (m s^{-1})	σ_{Dif} (m s^{-1})	σ_{ur1} (m s^{-1})	σ_{ur2} (m s^{-1})
M8	0.076	0.078	0.0096	0.033	0.070
M3	0.083	0.084	0.0070	0.036	0.076
M7	0.039	0.039	0.0067	0.023	0.031

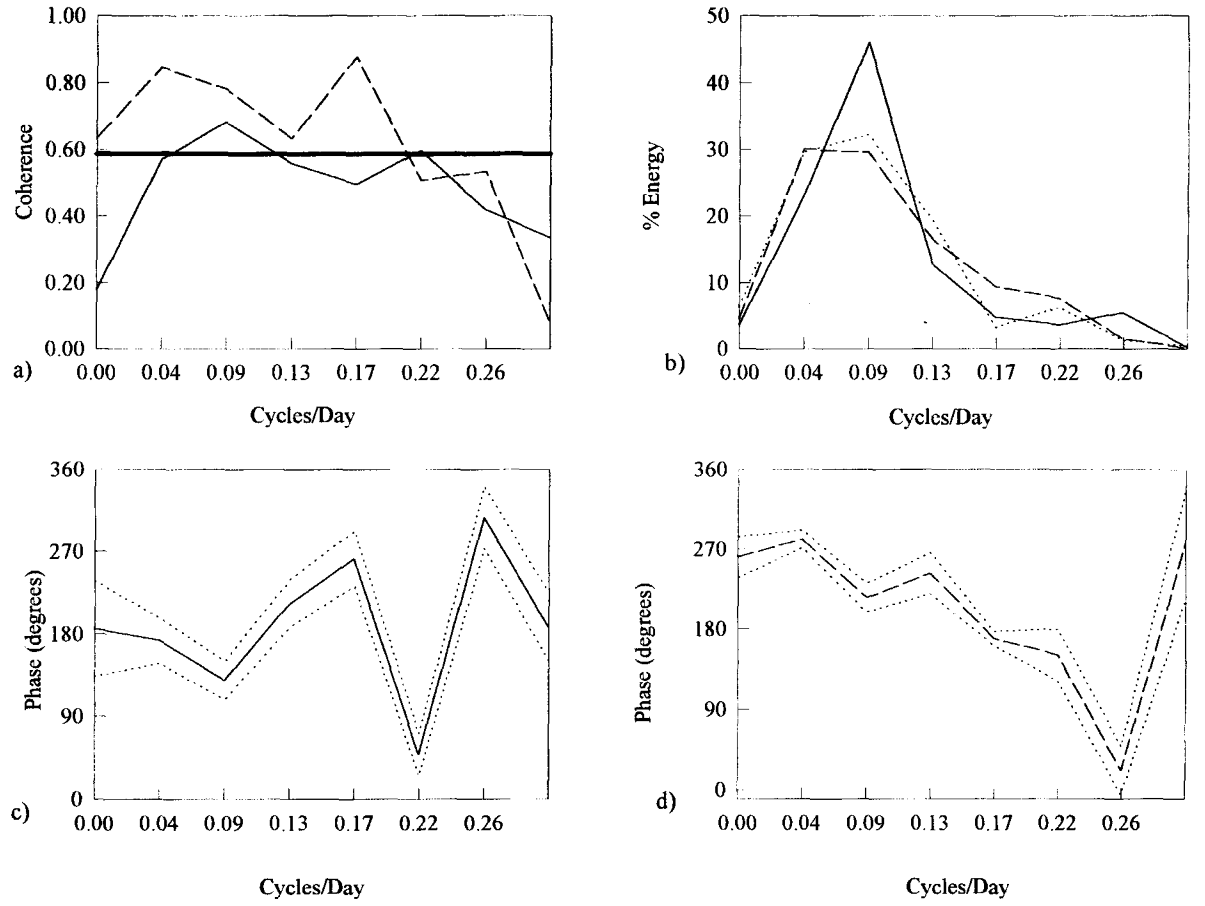

Figure 3

Results of the cross-spectral analysis between $U_m(t)$, $\phi_m(t)$ series and $M_1(t)$ series at mooring M8. a) coherence diagram $U_m(t)$ vs $M_1(t)$ and $\phi_m(t)$ vs $M_1(t)$ (dashed line), horizontal line means for 95% significant level for coherence in accordance with Box and Jenkins (1970) b) percentage of variance explained for each frequency band $U_m(t)$ (solid line) ϕ_m (1) (dashed line) and $M_1(t)$ (dotted line); c) phase diagram, cross between $M_1(t)$ and $U_m(t)$ d) phase diagram, cross between $M_1(t)$ and $\phi_m(t)$. Spectral estimations have been done with nine degrees of freedom and the band width used was $\Delta\omega = 0.0432$ cycles/day, confidence intervals for phases were obtained in accordance with Box and Jenkins (1970).

where

$$C_0 = U_{M_2}(U_t - 1)$$

explaining the contribution to semidiurnal residue by the amplitude variations; the second one is proportional to an orthogonal phase-lag signal with respect to the M_2 one:

$$u_{r_2} = S_0 \sin(\omega_{M2} t - \delta_{u_{M2}}) \quad (7)$$

where

$$S_0 = \delta_{uM2} U_{M_2}(\phi_t - 1)$$

for the contribution to semidiurnal residue by the phase-lag variations. The different contributions to semidiurnal residue from amplitude and phase-lag variations on the M_2 signal can thus be evaluated. The u_{r1} and u_{r2} series obtained from mooring M3 are shown in Figures 6*d* and 6*e*, respectively.

The standard deviation of the residues computed from equations (2) and (5) and of the M_2 signal amplitude and phase variation contributions from equations (6) and (7) are shown in Table 5. The residual signal is higher at mooring M3, like the M_2 tidal signal (Table 3) showing at mooring M7 a reciprocal behaviour with the lower values. At mooring M8, values are close to those of mooring M3. Western-side moorings have a contribution of phase-lag variation to the residual signal almost double that of the amplitude variation. At mooring M7 the ratio between these contributions is close to unity.

SECOND-ORDER QUASI-ANALYTICAL SOLUTION FOR THE NON-LINEAR INTERACTION BETWEEN TIDAL AND SUBINERTIAL BAROTROPIC OSCILLATIONS

To explain this relationship between amplitude and phase variation of M2 and the barotropic signal in the current

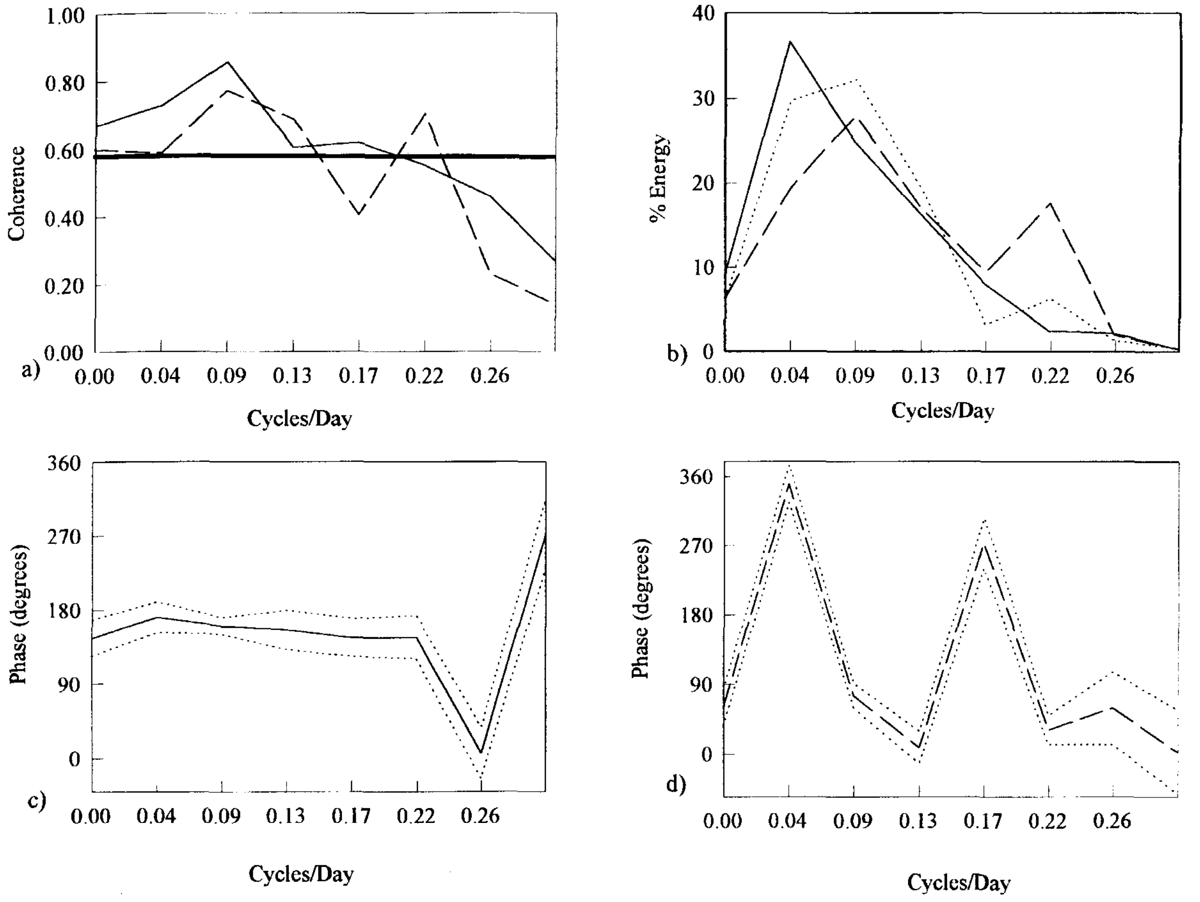

Figure 4

Results of the cross-spectral analysis between $U_m(t)$, $\phi_m(t)$ series and $M_1(t)$ series at mooring M8. a) coherence diagram $U_m(t)$ vs $M_1(t)$ and $\phi_m(t)$ vs $M_1(t)$ (dashed line), horizontal line means for 95% significant level for coherence in accordance with Box and Jenkins (1970) b) percentage of variance explained for each frequency band $U_m(t)$ (solid line) $\phi_m(1)$ (dashed line) and $M_1(t)$ (dotted line); c) phase diagram, cross between $M_1(t)$ and $U_m(t)$ d) phase diagram, cross between $M_1(t)$ and $\phi_m(t)$. Spectral estimations have been done with nine degrees of freedom and the band width used was $\Delta\omega = 0.0432$ cycles/day, confidence intervals for phases were obtained in accordance with Box and Jenkins (1970).

velocity, non-linear interaction between subinertial and semidiurnal signals in the flow will be proposed as the responsible physical mechanism. A second-order solution characterizing this type of non-linear interaction can be established after considering the following:

a) A barotropic 1D flow along the longitudinal x axis of the Strait is assumed. The current velocity in the longitudinal direction is thus characterized by a cross-strait averaged value. Also, sea elevation ζ is assumed to be constant in the cross-strait direction, and is characterized by a cross-strait averaged value. The Coriolis-term effect on the longitudinal momentum balance is considered to be contained in these averaged values.

b) The bottom friction term is disregarded because of the high cross-strait averaged depth values (Mañanes, 1996).

c) The Strait geometry is treated as an ideal channel of variable rectangular section along the longitudinal coordinate x, $A = bh$ being the area of the section, where b is breadth and h is the effective depth (the cross-strait averaged depth).

d) $h+\zeta = h$ is assumed in the mass conservation equation.

e) The subinertial oscillation in the flow is assumed to behave as a simple harmonic of frequency ω_1.

f) The semidiurnal residue u_r arises exclusively from linear interaction between the subinertial and M_2 signals in the flow.

According to these assumptions, the equations for momentum and mass balances can be expressed as:

$$\frac{\partial u}{\partial t} + u\,\frac{\partial u}{\partial x} = -g\,\frac{\partial \zeta}{\partial x} \tag{8}$$

$$\frac{\partial (Au)}{\partial x} = -b\,\frac{\partial \zeta}{\partial t} \tag{9}$$

Next, the variables ζ and u are expanded using perturbation techniques as a power series of the small parameter $\varepsilon = \zeta/h$

$$\zeta = \varepsilon\,\bar{\zeta}_f + \varepsilon^2\,\bar{\zeta}_s + \dots \tag{10}$$

$$u = \varepsilon\,\bar{u}_f + \varepsilon^2\,\bar{u}_s + \dots \tag{11}$$

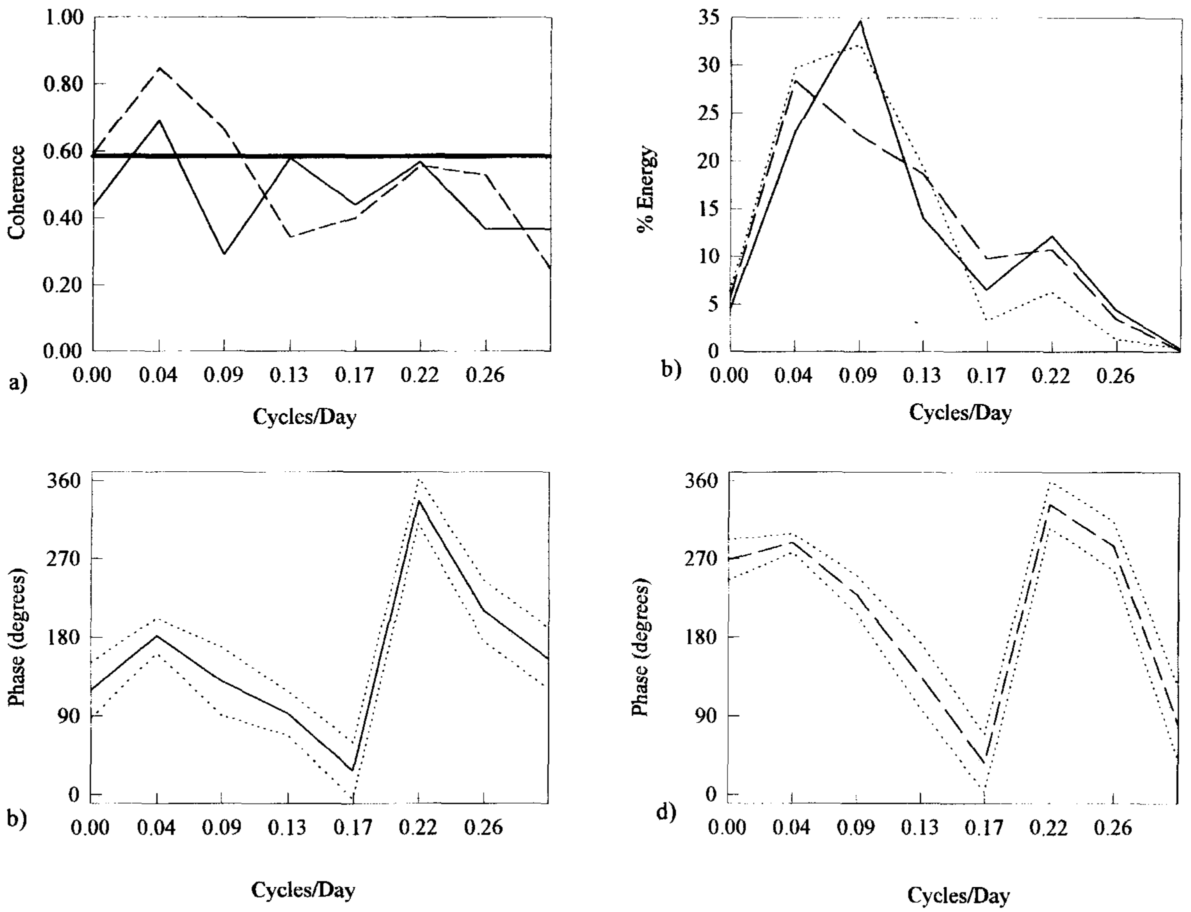

Figure 5

Results of the cross-spectral analysis between $U_m(t)$, $\phi_m(t)$ series and $M_1(t)$ series at mooring M8. a) coherence diagram $U_m(t)$ vs $M_1(t)$ and $\phi_m(t)$ vs $M_1(t)$ (dashed line), horizontal line means for 95% significant level for coherence in accordance with Box and Jenkins (1970) b) percentage of variance explained for each frequency band $U_m(t)$ (solid line) $\phi_m(1)$ (dashed line) and $M_1(t)$ (dotted line); c) phase diagram, cross between $M_1(t)$ and $U_m(t)$ d) phase diagram, cross between $M_1(t)$ and $\phi_m(t)$. Spectral estimations have been done with nine degrees of freedom and the band width used was $\Delta\omega = 0.0432$ cycles/day, confidence intervals for phases were obtained in accordance with Box and Jenkins (1970).

of which only the first two terms will be considered, implying that the solution to equations (8) and (9) consists of a first-order solution, $\zeta_f = \varepsilon\,\bar{\zeta}_f$ and $u_f = \varepsilon\,\bar{u}_f$; plus a second-order one, $\zeta_s = \varepsilon^2\,\bar{\zeta}_s$ and $u_s = \varepsilon^2\,\bar{u}_s$. It will now be assumed that the first-order terms in equations (10) and (11) are composed of

$$\zeta_f = \zeta_{M2} + \zeta_1 \tag{12}$$

$$u_f = u_{M2} + u_1 \tag{13}$$

i.e. by M_2 plus a subinertial signal, u_1 and ζ_1.

Taking equations (12) and (13) into equations (8) and (9) and neglecting terms with powers of ε greater than two, the following system of equations accounting for the effects of non-linear interaction between u_{M2} and u_1 variables is obtained

$$\frac{\partial u_s}{\partial t} + u_{M2}\,\frac{\partial u_1}{\partial x} + u_1\,\frac{\partial u_{M2}}{\partial x} = -g\,\frac{\partial \zeta_s}{\partial x} \tag{14}$$

$$\frac{\partial\,(A u_s)}{\partial x} = -b\,\frac{\partial \zeta_s}{\partial t} \tag{15}$$

the first stands for the momentum balance and the second for mass conservation and where the first-order solutions for current velocity associated to the interacting oscillations are characterized as

$$u_{M2} = U_{M2}(x)\,\cos\left[\omega_{M2}\,t - \delta_{uM2}(x)\right] \tag{16}$$

$$u_1 = U_1(x)\,\cos\left[\omega_1\,t - \delta_{u1}(x)\right] \tag{17}$$

$U_{M2}(x)$ and $U_1(x)$ being the amplitudes of M_2 and subinertial oscillations and $\delta_{uM2}(x)$ and $\delta_{u1}(x)$ their phase lags. All of them, amplitudes and phase lags, are functions of the spatial x co-ordinate.

Substituting the first-order solutions given by equations (16) and (17) into equation (14) and operating with

Figure 6

Temporal series of the semidiurnal residue in the current velocity at mooring M3. a) semidiurnal residue obtained from equation (2) $u_r\ (t)$; b) semidiurnal residue approximation from equation (5) $u_{ra}\ (t)$; c) difference between the residues of cases a) and b) $u_r\ (t) - u_{ra}\ (t)$; d) contribution to the semidiurnal residue from the M_2 signal amplitude variation $r_{r1}\ (t)$; e) contribution to the semidiurnal residue from the M_2 signal phase variation $u_{r2}\ (t)$.

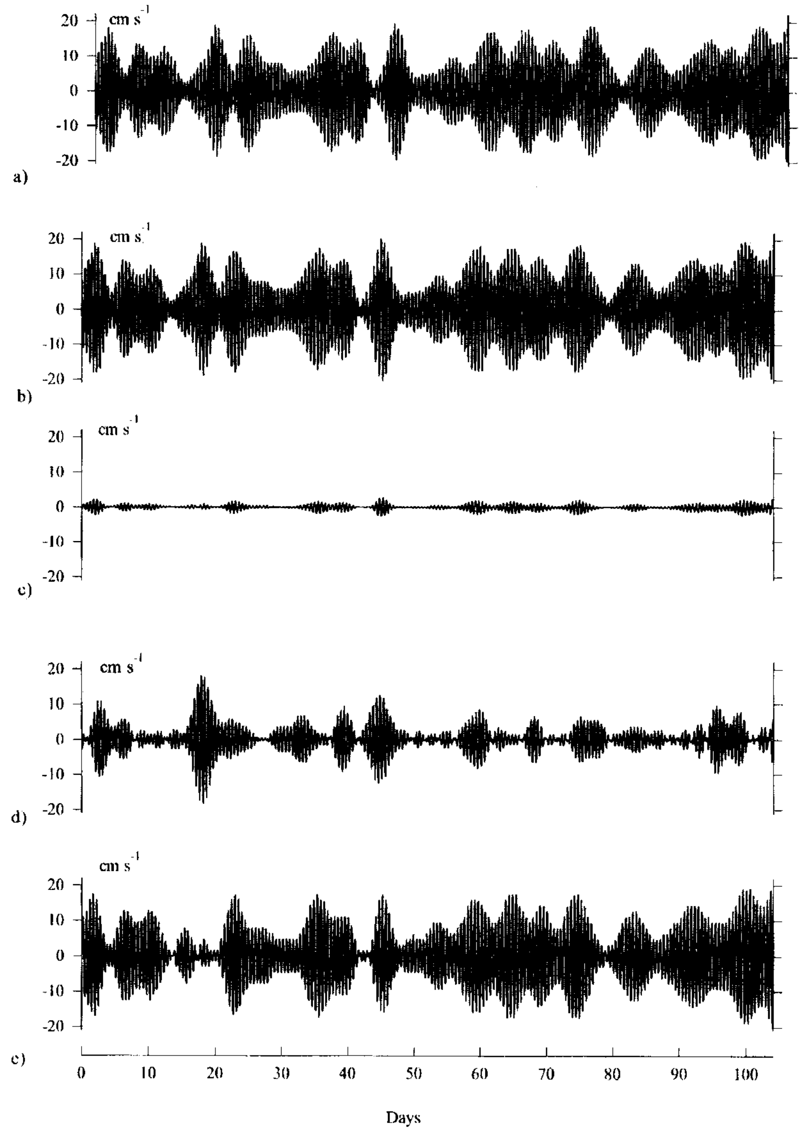

equation (15), the following differential equation for sea-level second-order solution ζ_s is obtained

$$\begin{aligned}
&\frac{\partial^2 \zeta_s}{\partial x^2} - \gamma \frac{\partial \zeta_s}{\partial x} - \frac{1}{gh}\frac{\partial^2 \zeta_s}{\partial t^2} \\
&= B_1 \cos\left[(\omega_{M2} - \omega_1)\, t - (\delta_{uM2} - \delta_{u_1})\right] \\
&+ B_2 \sin\left[(\omega_{M2} - \omega_1)\, t - (\delta_{uM2} + \delta_{u_1})\right] \\
&+ B_3 \sin\left[(\omega_{M2} - \omega_1)\, t - (\delta_{uM2} - \delta_{u_1})\right] \\
&+ B_4 \sin\left[(\omega_{M2} + \omega_1)\, t - (\delta_{uM2} + \delta_{u_1})\right] \qquad (18)
\end{aligned}$$

where the coefficients B_i are expressed as:

$$B_1 = \left[\frac{\gamma A}{2} + E + \frac{\gamma D}{2} + H\right]$$

$$B_2 = \left[\frac{\gamma A}{2} + E + \frac{\gamma D}{2} - H\right]$$

$$B_3 = \left[-\frac{\gamma B}{2} - F + \frac{\gamma C}{2} + G\right]$$

$$B_4 = \left[\frac{\gamma B}{2} + F + \frac{\gamma C}{2} + G\right]$$

and

$$A = \frac{U_{M2}\, U_1'}{2g}; \quad B = \frac{U_{M2}\, \delta_{u1}'\, U_1}{2g}$$

$$C = \frac{U_1\, \delta_{uM2}'\, U_{M2}}{2g}; \quad D = \frac{U_1\, U_{M2}'}{2g}$$

$$E = \frac{U_{M2}'\, U_1}{g}; \quad F = \frac{U_{M2}'\, \delta_{u1}\, U_1}{g}$$

$$G = \frac{U_1'\, \delta_{uM2}'\, U_{M2}}{g}; \quad H = \frac{\delta_{u1}'\, U_1\, U_{M2}\, \delta_{uM2}'}{g}$$

γ parameter is defined as $\gamma = (1/A)(dA/dx)$ and apostrophe ' means derivatives with respect to x coordinate. Thus, coefficients B_i are functions of; U_{M2}, U_1, U_{M2}', U_1', δ_{uM2}', δ_{u1}' and γ parameter.

If solution ζ_s is evaluated between two sections separated by a small enough distance, then it can be assumed that:

$$B_i,\ U'_{M2},\ U'_1,\ \delta'_{uM2},\ \delta'_{u1}\ \gamma = \text{constants}$$

that is, the amplitudes, phase lags and area of the sections can be assumed to behave following a linear variation along x axis. After solution ζ_s is obtained under this assumption, its substitution in equation (8) leads to the following second-order solution for current velocity u_s

$$u_s = C_m\ \cos(\omega_{M2}\, t - \delta_{u_{M2}}) + S_m \sin(\omega_{M2}\, t - \delta_{u_{M2}}) \tag{19}$$

where

$$C_m = X_c \cos(\omega_1\, t - \delta_{u_1} + \varphi_{cm}) \tag{20}$$

$$S_m = X_s \cos(\omega_1\, t - \delta_{u_1} + \varphi_{sm}) \tag{21}$$

are time-dependent coefficients, which can be understood as low-frequency harmonics of the same frequency as subinertial oscillation. The constants X_c and X_s represent the theoretical contribution of the amplitude and phase modulations of the M_2 signal, respectively, to the amplitude of the non-linearly generated semidiurnal residue. The constants φ_c and φ_s represent the phase lag between the modulation of amplitude and phase of the M_2 signal with respect to subinertial flow. These constants are functions of ω_{M2}, ω_1, U_{M2}, U_1, U'_{M2}, U'_1, δ'_{uM2}, δ'_{u1} and γ in the following manner:

$$X_c = \sqrt{R_1^2 + R_2^2}, \quad \varphi_{Cm} = \arctan\left(-\frac{R_2}{R_1}\right)$$
$$X_s = \sqrt{R_3^2 + R_4^2}, \quad \varphi_{Sm} = \arctan\left(-\frac{R_3}{R_4}\right)$$

where

$$R_1 = \left[-\frac{Z_3}{(\omega_{M2} - \omega_1)} - \frac{Z_4}{(\omega_{M2} + \omega_1)}\right]$$
$$R_2 = \left[\frac{Z_2}{(\omega_{M2} + \omega_1)} - \frac{Z_1}{(\omega_{M2} - \omega_1)}\right]$$
$$R_3 = \left[\frac{Z_1}{(\omega_{M2} - \omega_1)} + \frac{Z_2}{(\omega_{M2} + \omega_1)}\right]$$
$$R_4 = \left[-\frac{Z_3}{(\omega_{M2} - \omega_1)} + \frac{Z_4}{(\omega_{M2} + \omega_1)}\right]$$

and

$$Z_1 = (\delta'_{uM2} - \delta'_{u1})\, g\, (G_3 \cos\varphi_1 - G_1 \sin\varphi_1) + \frac{A+D}{2}$$
$$Z_2 = (\delta'_{uM2} + \delta'_{u1})\, g \sin\varphi_1\, (G_4 - G_2) + \frac{A+D}{2}$$
$$Z_3 = -(\delta'_{uM2} - \delta'_{u1})\, g\, (G_3 \sin\varphi_1 + G_1 \cos\varphi_1) + \frac{C-B}{2}$$
$$Z_4 = (\delta'_{uM2} + \delta'_{u1})\, g \cos\varphi_2\, (G_4 - G_2) + \frac{B+C}{2}$$

being given G_i and φ_i as

$$G_1 = \frac{B_1}{S_1}; \quad G_2 = \frac{B_2}{S_2}$$
$$G_3 = \frac{B_3}{S_1}; \quad G_4 = \frac{B_4}{S_2}$$
$$\varphi_1 = \arctan(T_1)$$
$$\varphi_2 = \arctan(T_2)$$

with

$$S_1 = \sqrt{\left[(\delta'_{uM2} - \delta'_{u1})^2 - \frac{(\omega_{M2} - \omega_1)^2}{gh}\right]^2 + \gamma^2 (\delta'_{uM2} - \delta'_{u1})^2}$$
$$S_2 = \sqrt{\left[(\delta'_{uM2} + \delta'_{u1})^2 - \frac{(\omega_{M2} + \omega_1)^2}{gh}\right]^2 + \gamma^2 (\delta'_{uM2} - \delta'_{u1})^2}$$

$$T_1 = \frac{\gamma\,(\delta'_{uM2} - \delta'_{u1})}{(\delta'_{uM2} - \delta'_{u1})^2 - \frac{(\omega_{M2} - \omega_1)^2}{gh}}$$
$$T_2 = \frac{\gamma\,(\delta'_{uM2} + \delta'_{u1})}{(\delta'_{uM2} + \delta'_{u1})^2 - \frac{(\omega_{M2} - \omega_1)^2}{gh}}$$

The structure of the solution given by equation (19) is presented in a identical manner to the expression for semidiurnal residue given for equation (5). Therefore, if this semidiurnal residue is the result of the described non-linear mechanism, $u_r = u_s$ then the behaviour of the observed time-dependent coefficients C_0 and S_0 must be similar to that showed by the theoretical ones C_m and S_m.

To compare the observed series C_0 and S_0 with the theoretical ones C_m and S_m, the solution given by equation (19) will be evaluated at half-distance between the sections corresponding to moorings M8 and M3. The constants of the solution given by equation (19), X_c, X_s, φ_{cm} and φ_{sm}, are functions of the quantities ω_{M2}, U_{M2}, U'_{M2}, and δ'_{uM2}, associated to the M_2 signal, and ω_1, U_1, U'_1 and δ'_{u1}, associated to the subinertial oscillation. An estimation of the quantities U_{M2}, U'_{M2}, and δ'_{uM2}, U_1, U'_1 can be given if it is supposed that the current-velocity measurements at moorings M3 and M8 are representative for the cross-strait averaged current velocity. As the solution given by equation (19) will be constructed on the above parameters, estimated from the observed current-velocity series, the result will be a quasi-analytical solution.

The parameters associated to the M_2 signal, of angular frequency $\omega_{M2} = 1.4 \times 10^{-4}\,\mathrm{rad\,s^{-1}}$, can be estimated from Table 3, with a distance between moorings M8 and M3 of 10 km and assuming a linear variation of current-velocity amplitude between these moorings. Thus the values, $U_{M2} = 0.77\ \mathrm{m.s^{-1}}$ (the mean value between moorings M3 and M8) and $U'_{M2} = 2.5 \times 10^{-5}\,\mathrm{s^{-1}}$ are obtained. Taking into consideration that the phase lag of the M_2 signal in sea elevation varies very slightly in the along-Strait co-ordinate (García, 1986; Candela, 1989) a value $\delta'_{uM2} = 0$ is also assumed for the current velocity phase lag.

As more than 90% of the subinertial current variance, moorings M8 and M3, was explained by the barotropic mode during the subperiod from 3 December 1985 to 11 January 1986, this was selected to extract the estimates to the associated subinertial signal parameters. A series of depth-averaged values of the subinertial signals from the three current meters of mooring M3 (after removing the mean values of the series) is thus taken to characterize the barotropic subinertial signal in the M3 section. It is further assumed that the M8 subinertial signal is representative for the barotropic subinertial signal in the M8 section.

Once the barotropic subinertial current velocity series have been obtained for the selected subperiod, the parameters associated to the subinertial current oscillation can be estimated via the cross spectral analysis between the subinertial signals at moorings M8 and M3.

From this cross-analysis, we obtain the modulus of the transfer function and phase lag for the three frequencies whose barotropic subinertial variance was higher (*see* section 2). They are the same for the subperiod used. From these results, *see* Table 6; U'_1 and δ'_{u1} can be estimated giving a distance between moorings M8 and M3, $L = 10$ km, and using the transfer function modulus, $Z(\omega_1)$, and phase lags, $\varphi(\omega_1)$, values:

$$U'_1(\omega_1) = \frac{U_{1M3}(\omega_1) - U_{1M8}(\omega_1)}{L}$$
$$U_{1M3}(\omega_1) = Z(\omega_1)\, U_{1M8}(\omega_1)$$
$$\delta'_{u1}(\omega_1) = \frac{\varphi(\omega_1)}{L}$$

where $U_{1M8}(\omega_1)$ and $U_{1M3}(\omega_1)$ are the amplitudes of the subinertial oscillations for each frequency which are obtained by

$$U_{1M8}(\omega_1) = [S_{M8}(\omega_1)\,\Delta\omega]^{1/2}$$
$$U_{1M3}(\omega_1) = [S_{M3}(\omega_1)\,\Delta\omega]^{1/2}$$

Table 6

Results of cross-spectral analysis between the subinertial signal at moorings M8 and M3 for the period from 15 November 1985 to 25 December 1985 and estimation of the parameters U_1, U'_1 and δ'_{u1}.

Frequency (cycle/day)	Coherence	$Z(\omega_1)$	$U_1(\omega_1)$ (m s^{-1})	$U'_1(\omega_1)$ (s^{-1})	$\delta'_{u1}(\omega_1)$ (rad m^{-1})
0.0432	0.83	1.61	0.06	3.7 10^{-6}	−1.6 10^{-4}
0.0864	0.95	1.60	0.11	5.3 10^{-6}	−4.7 10^{-5}
0.1296	0.97	1.53	0.05	2.2 10^{-6}	1.0 10^{-5}

where $S_{M8}(\omega_1)$ and $S_{M8}(\omega_1)$ are the spectral densities of the subinertial signal at each mooring and $\Delta\omega$ is the band width used in the cross-spectral analysis, $\Delta\omega = 0.0432$ cycles/day. Proceeding in this fashion, the values for $U_1 = (U_{1M8} + U_{1M3})/2$, U'_1 and δ'_{u1} presented in the last columns of Table 6 are obtained.

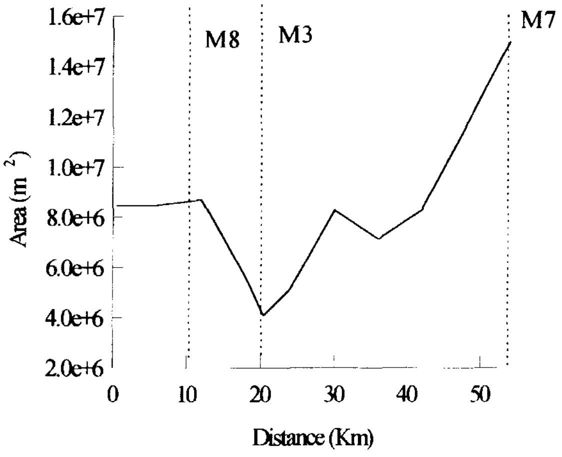

Figure 7

Cross-section area variation along the Strait of Gibraltar. Vertical dotted lines indicate locations of moorings M8, M3 and M7.

Once the parameters associated to the interacting first-order oscillations are obtained, and after taking the value of $\gamma = -7.5\,10^{-5}$ (*see* Figure 7 where the area variations of the ideal rectangular sections along the Strait are shown), and $h = 200$ m as the mean depth between moorings M8 and M3, the constants of the solution (eq. (19)) can be evaluated. Since the theoretical solution has a very slight dependence on the frequency ω_1 in the range from 0.0432 to 0.1296 cycles/day, a first idea about how this solution is behaving can be achieved by evaluation at a medium frequency $\omega_1 = 0.0864$ cycles/day through different values U_1, U'_1 and δ'_{u1}. To perform these computations an averaged value of admittance $\bar{Z}(\omega_1)$ along the three frequencies from Table 6 is taken. Once this value is established, the following relation between the parameters U_1 and U'_1 is obtained

$$U'_1 = \frac{2\,[\bar{Z}(\omega_1) - 1]}{[\bar{Z}(\omega_1) + 1]\,L}\, U_1$$

Under these conditions, the theoretical solution now depends only on two parameters U_1 and δ'_{u1}. Thus the theoretical solution is evaluated through the values U_1 running from 0.01 to 0.40 m s^{-1} each $\Delta U_1 = 0.01\,\mathrm{m\,s^{-1}}$ and through the values for δ'_{u1} from $-10^{-4}\,\mathrm{rad\,m^{-1}}$ each $\Delta\delta'_{u1} = 10^{-6}\,\mathrm{rad\,m^{-1}}$. The limits of the δ'_{u1} values correspond to a phase lag between the two sections, that when they are translated to time, given the value $\omega_1 = 0.0864$ cpd, they represent a maximum time delay of 1.84 days.

The values for the constants X_c, X_s, φ_c and φ_s resulting from these computations are shown in Figures 8 and 9.

It can be seen that both X_c and X_s increase when the amplitude of subinertial current velocity U_1 increases. When δ'_{u1} is zero, a zero value for X_c is obtained while significant values of X_s can still be produced. In general, X_c has a stronger dependence on δ'_{u1} than on X_s.

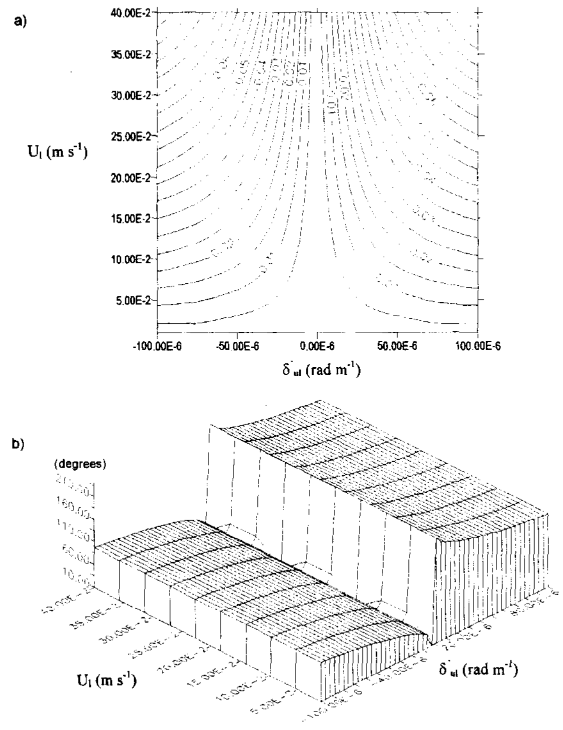

Figure 8

Constants X_c and φ_{cm} of the quasi-analytical solution given by equation (19) through different values of U_1 and δ'_{u1} and for a value of ω_1 = 0.0864 cycles/day. a) X_c in m s^{-1}; b) φ_{cm} in degrees.

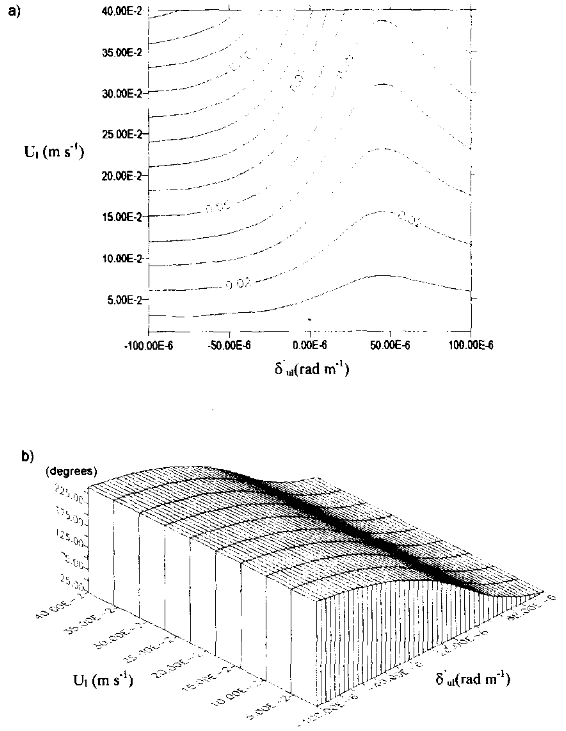

Figure 9

Constants X_c and φ_{cm} of the quasi-analytical solution given by equation (19) through different values of U_1 and δ'_{u1} and for a value of ω_1 = 0.0864 cycles/day. a) X_c in m s^{-1}; b) φ_{cm} in degrees.

The phase lags of the variations in amplitude and phase of the M_2 signal with respect to the subinertial signal φ_c and φ_s, depend only on δ'_{u1} and maintain a constant value along the different values of U_1. For negative δ'_{u1} values, φ_c lies between 0 and 100° and φ_s between 180 and 260° while for positive values φ_c is between 180 and 240 and φ_s between 0 and 180°. In these results, the variable δ'_{u1} plays an important role in determining the phase lag of modulations in amplitude and phase of the M_2 signal with respect to subinertial flow.

COMPARISON BETWEEN THE THEORETICAL SOLUTION AND THE OBSERVED RESULTS

In this part, the theoretical results, based on the quasi-analytical solution obtained in the previous section, will be compared with the observed results obtained at mooring M3. Using the results of Table 6 (obtained for the subperiod from 3 December 1985 to 11 January 1986) the previous solution is evaluated for each of the frequencies where the major part of the variance of both subinertial oscillation and variations in amplitude and phase of the M_2 signal was contained. These were: ω_1 = 0.0432, 0.0864, 0.1296 cycles/day.

In each of these frequencies the behaviour of the observed series C_0 and S_0 given in equations (6) and (7) is compared with the theoretical series C_m and S_m given by equations (20) and (21). In order to perform this comparison, the variances in each frequency of the observed series are computed as:

$$V_{C_0}(\omega_1) = S_{C0}(\omega_1)\,\Delta\omega$$
$$V_{S0}(\omega_1) = S_{S0}(\omega_1)\,\Delta\omega$$

where $S_{C0}(\omega_1)$ and $S_{S0}(\omega_1)$ are the spectral densities of series C_0 and S_0, respectively: and $\Delta\omega$ = 0.0018 cycles/day is the band width used in the spectral estimations. Next, the phase lag of C_0 and S_0 series with respect to the subinertial signal u_1 are computed via cross-spectral analysis and defined as φ_{C0} and φ_{S0}, respectively.

On the other hand, the variances of the theoretical series C_m and S_m in each frequency are defined as

$$V_{Cm}(\omega_1) = [X_c(\omega_1)]^2$$
$$V_{Sm}(\omega_1) = [X_s(\omega_1)]^2$$

and their phase lags with respect to subinertial signal as in equations (20) and (21).

All of the above quantities are presented in Table 7 for each of the three frequencies, together with the value of coherence among the subinertial flow and the C_0 and S_0 series.

Table 7

Comparison between observed C_0 and S_0 (from mooring M3) and theoretical, C_m and S_m, series. Second column shows the coherence values obtained from the spectral cross of series C_0 and S_0 with the subinertial oscillation in the current velocity (at mooring M3). a) Values for C_0 and C_m. b) Values for S_0 and S_m.

a)

Frequency (cycles/day)	Coherence	V_{Co} ($cm^2\ s^{-2}$)	V_{Cm} ($cm^2\ s^{-2}$)	φ_{Co} (degrees)	φ_{Cm} (degrees)
0.0432	0.65	5.71	2.56	147	108
0.0864	0.83	12.60	2.82	121	73
0.1296	0.61	3.61	0.06	225	226

b)

Frequency (cycles/day)	Coherence	V_{So} ($cm^2\ s^{-2}$)	V_{Sm} ($cm^2\ s^{-2}$)	φ_{So} (degrees)	φ_{Sm} (degrees)
0.0432	0.46	3.92	3.96	270	280
0.0864	0.93	10.00	11.00	209	234
0.1296	0.23	2.62	1.02	164	178

From Table 7, it can be seen that the theoretical results are in good agreement with the observed ones in those frequencies where the coherence between the subinertial flow and the C_0 and S_0 series is higher and where at the same time the major part of the variance is concentrated.

As to the comparison between C_m and C_0 series, their maximum variance is located at the frequency 0.0864 cycles/day, although the values for the observed series are much greater than the theoretical ones. The theoretical and observed values for the phase lag with respect to subinertial flow are agree quite well in all the three frequencies being close to 100° in the two first and having a value of 226° in the third one.

Concerning the S_m and S_0 series, their maximum variance is also located at the frequency 0.0864 cycles/day and here the values for the theoretical and observed series are fairly similar, as well as the values of their phase lag with respect to subinertial flow.

The theoretical results seem to be in better agreement with the observed ones in the case of S_m and S_0 at least for the two first frequencies where the coherence between subinertial flow and S_0 is also more significant.

It should be noted that despite of the strong restrictions under which the quasi-analytical solution has been obtained, it does seem to the able to describe a significant part of the investigated phenomenon. Therefore the variations in amplitude and phase lag of the M_2 signal in the current velocity can be partially explained by the proposed non-linear mechanism, interacting non-linearly with the tidal and subinertial flows through the advective term in the momentum balance equation.

In order to read this quasi-analytical result in a more intuitive physical frame, we can take as an example the φ_{cm} and φ_{cm} values corresponding to $\delta'_{u1} = 0$. In this case, from Figures 8 and 9 we have values close to 360° for φ_{cm} and 180° for φ_{sm}. The value of φ_{sm} means that when the subinertial flow is directed towards the Mediterranean ($u_1 > 0$), S_m, and therefore ϕ_t, decreases with a time ahead in the occurence of the tidal current velocity maximum. When the subinertial flow is towards the Atlantic ($u_1 < 0$), the inverse situation with a time delay in the occurence of the tidal current maximum is produced. On the other hand, a φ_{cm} close to 360° means that when $u_1 > 0$ or $u_1 < 0$ the tidal current amplitude increases or decreases.

In terms of tidal propagation through isophase and isoamplitude lines of the tidal current velocity (Mañanes, 1996), the above result could be translated into a displacement of these along the Strait direction (east or west) according to the subinertial flow direction. The larger the subinertial flow, the larger this displacement.

Finally, the authors wish to point out that the results obtained are only referred to the western side of the Strait. Further measurements and analyses are needed to investigate the way in which this non-linear interaction affects the tidal signal on the eastern side.

Acknowledgements

The authors wish to thank Julio Candela, Antonio Ruiz-Cañavate and Juan Rico for their helpful comments on this work, which was supported by CYCIT Project No AMB94-0591.

REFERENCES

Box G.E.P. and G.M. Jenkins (1970). *Time series analysis, forecasting and control.* Holden day, Inc. San Francisco.

Bruno M.R., R. Mañanes, J.J. Alonso, L. Tejedor (1996*a*). Meteorological tides and relationship with semidiurnal residues. *Sci. Mar.* **60(4)**, 451-459.

Bruno M., B. Fraguela, J.J. Alonso, R. Mañanes, A. Ruíz, J. Rico (1996*b*). The use of EOF in the analysis of mean sea level. An application to Cadiz. *Int. Hydrogr. Rev.* **73**, 99-107.

Bruno M. (1993). Un análisis de las causas que contribuyen a la distorsión de la señal semidiurna de marea en la costa este de la isla de Gran canaria. *Ph. D. Thesis*, Universidad de Cádiz.

Bryden H.L., J. Candela, T. Kinder (1994). Exchange through the Strait of Gibraltar. *Prog. Oceanogr.* **33**, 201-248.

Candela J., C.D.. Winant, A. Ruíz (1990). Tides in the Strait of Gibraltar. *J. Geophys. Res.* **95**, 7317-7335.

Candela J., C.D. Wianant, H.L. Bryden (1989). Meteorologically forced subinertial flows through the Strait of Gibraltar. *J. Geophys. Res.* **94**, 12667-12674.

Candela J. (1989). Tidal and subinertial flows through the Strait of Gibraltar. *Ph. D. Thesis*, S.O.I., La Jolla, California.

Crépon M. (1965). Influence de la pression atmosphérique sur le niveau moyen de la Méditerranée Occidentale et sur le flux à travers le détroit de Gibraltar. *Cah. Oceanogr.* **1**, 15-23.

Foreman M.G.G. (1976). Manual for tidal heights and prediction. Pacific Marine Sciences report 77-10. *Inst. Ocean of Sciences, Patrice Bay.*

García J.M. (1986). Variabilidad del nivel del mar en el Estrecho de Gibraltar: Marea y oscilaciones residuales. *Ph. D. Thesis*, Universidad de Málaga.

Garret C., J. Akerly, K. Thompson (1989). Low frequency fluctuations in the Strait of Gibraltar from MEDAPLEX sea level data. *J. Phys. Oceanogr.* **19**, 1682-1696.

Godin G. (1972). *The analysis of tides.* University of Toronto, Toronto.

Korn G.A. and T.M. Korn (1986). *Mathematical handbook for scientists and engineers.* Mc Graw-Hill, 1130.

Kundu P.K., J.S. Allen, R.L. Smith (1975). Modal decomposition of the velocity field near the Oregon coast. *J. Phys. Oceanogr.* **5**, 683-704.

Kundu P.K. and J.S. Allen (1976). Some three-dimensional characteristics of low-frequency current fluctuations near the Oregon coast. *J. Phys. Oceanogr.* **5**, 181-200.

Lacombe H. and C. Richez (1982). The regime of Strait of Gibraltar. In *Hydrodynamics of semi-enclosed seas*, J.C.J. Nihoul Ed., Elsevier Sci. Publ. Comp., New York, 13-73.

Mañanes R., M. Bruno, J. Rico (1995). Un estudio de las variaciones de corto periodo de la onda M_2 en el Estrecho de Gibraltar. *VII Asemblea Nacional de Geofísica, Sesiíon de Oceanografía*, 130.

Mañanes R. (1996). Interacción no lineal entre los flujos subinerciales y mareales asociados al régimen barotrópico en el Estrecho de Gibraltar. *Ph. D. Thesis*, Universidad de Cádiz.

Pillsbury R.D., D. Barstow, J.S. Botero, C. Millero, B. More, G. Pittock, D.C. Root, J. Simpkims III., R.E. Still, H.L. Bryden (1987). Gibraltar Experiment: current measurements in the Strait of Gibraltar. *Oregon State University Technical report* **87**, 29-284.

Ruíz A. (1994). Flujos barotrópicos de marea en el Estrecho de Gibraltar. *Ph. D. Thesis*, Universidad de Cádiz.